Draft version September 28, 2016
Preprint typeset using LaTeX style AASTeX6 v. 1.0

arXiv:1609.08290v1 [astro-ph.HE] 27 Sep 2016

CENTRAL ENGINE OF LATE-TIME X-RAY FLARES WITH INTERNAL ORIGIN

Hui-Jun Mu[1], Wei-Min Gu[1], Shu-Jin Hou[2], Tong Liu[1,4], Da-Bin Lin[3], Tuan Yi[1], En-Wei Liang[3], and Ju-Fu Lu[1]

[1]Department of Astronomy and Institute of Theoretical Physics and Astrophysics, Xiamen University, Xiamen, Fujian 361005, China; guwm@xmu.edu.cn
[2]College of Physics and Electronic Engineering, Nanyang Normal University, Nanyang, Henan 473061, China
[3]GXU-NAOC Center for Astrophysics and Space Sciences, Department of Physics, Guangxi University, Nanning 530004, China
[4]Department of Physics and Astronomy, University of Nevada, Las Vegas, NV 89154, USA

ABSTRACT

This work focuses on a sample of seven extremely late-time X-ray flares with peak time $t_{\rm p} > 10^4$s, among which two flares can be confirmed as the late-time activity of central engine. The main purpose is to investigate the mechanism of such late-time flares based on the internal origin assumption. In the hyper-accreting black hole (BH) scenario, we study the possibility of two well-known mechanisms as the central engine to power such X-ray flares, i.e., the neutrino-antineutrino annihilation and the Blandford-Znajek (BZ) process. Our results show that the annihilation luminosity is far below the observational data. Thus, the annihilation mechanism cannot account for such late-time flares. For the BZ process, if the role of outflows is taken into consideration, the inflow mass rate near the horizon will be quite low such that the magnetic field will probably be too weak to power the observed X-ray flares. We therefore argue that, for the late-time flares with internal origin, the central engine is unlikely to be associated with BHs. On the contrary, a fast rotating neutron star with strong bipolar magnetic fields may be responsible for such flares.

Keywords: accretion, accretion disks — black hole physics — gamma-ray burst: general — magnetic fields — neutrinos

1. INTRODUCTION

In the past twenty years, great progress has been achieved on the understandings of gamma-ray bursts (GRBs). In particular, Swift has opened a new window to understand the nature of GRB phenomenon (e.g., Mészáros (2006); Zhang et al. (2007); Liang et al. (2010)). The onboard X-Ray Telescope (XRT; Burrows et al. 2005a) opened an exciting era for GRB researches. It has established a large sample of X-ray light curves from tens of seconds to days, sometimes even months (e.g., GRB 060729; Grupe 2006). It is interesting to find that X-ray flares are common in GRBs, which occur well after the initial prompt emission (Romano et al. 2006; Falcone et al. 2007; Chincarini et al. 2007; Margutti et al. 2010, 2011; Bernardini et al. 2011). X-ray flares have been observed both in long and short GRBs (Romano et al. 2006; Falcone et al. 2006; Campana et al. 2006; Margutti et al. 2011). Based on the observations from Swift/XRT, four power-law light-curve segments together with a flaring component are identified in the X-ray afterglow phase (Zhang et al. 2006; Nousek et al. 2006; O'Brien et al. 2006). The temporal analysis and spectral property suggest that the X-ray flare is from a distinct emission mechanism, since the temporal behavior of flares is quite similar to the prompt emission pulses, whereas different from the other four components in the canonical light-curves. Thus, X-ray flares may have a common physical origin as the prompt pulses (Burrows et al. 2005b; Falcone et al. 2006, 2007; Liang et al. 2006; Nousek et al. 2006; Zhang et al. 2006; Chincarini et al. 2007, 2010; Wu et al. 2013; Hou et al. 2014a; Yi et al. 2015), and are probably related to the late time activity of the central engine (Romano et al. 2006; Bernardini et al. 2011).

The central engine of GRBs remains an open question (Zhang 2011). A hyper-accreting stellar-mass black hole (BH) or a millisecond magnetar (Usov 1992; Dai & Lu 1998; Zhang & Mészáros 2001; Metzger et al. 2011) is usually invoked as possible GRB central engine. In the BH hyper-accretion scenario, the photons generated in the accretion flow can hardly escape due to the extremely large optical depth. On the contrary, a large amount of neutrinos can escape from the flow and therefore the neutrino cooling may be the most important mechanism to balance the viscous heating. Such a flow is named as the neutrino-dominated accretion flow (NDAF). The structure and

radiation of an NDAF has been extensively studied (e.g., Popham et al. (1999); Di Matteo et al. (2002); Gu et al. (2006); Kawanaka & Mineshige (2007); Liu et al. (2007, 2013, 2014); Lei et al. (2009); Zalamea & Beloborodov (2011); Pan & Yuan (2012); Janiuk et al. (2013); Xue et al. (2013); Cao et al. (2014). In the hyper-accretion scenario, the relativistic jet may be powered by the following two mechanisms. The first one is related to the annihilation of neutrino-antineutrino pairs. Such an annihilation process was previously investigated by several works (e.g., Popham et al. (1999); Di Matteo et al. (2002); Gu et al. (2006); Birkl et al. (2007); Liu et al. (2007); Xue et al. (2013); Liu et al. (2016). The second one is related to the Blandford-Znajek (BZ) process (Blandford & Znajek 1977), which can effectively extract the rotational energy of the central BH through large-scale magnetic fields.

The physical origin of X-ray flares remains mysterious, including internal dissipation and external shock mechanisms. Falcone et al. (2007) showed that many X-ray flares are from late-time activity of the internal engine that spawned the initial GRB, not from an afterglow-related effect. Moreover, Chincarini et al. (2010) and Margutti et al. (2010) made analyses of the flare temporal and spectral properties of a large sample of early-time flares and of a subsample of bright flares, which revealed close similarities between them and the prompt emission pulses, and therefore pointing to an internal origin. Margutti et al. (2011) investigated the relation between flares and continuum emission, and suggested the variability to be established as a consequence of different kinds of instabilities. On the other hand, from the theoretical view, Ioka et al. (2005) proposed a criterion to separate the internal and external origin of flares. Curran et al. (2008) concluded that the late-time flares ($t_{\rm p} \gtrsim 10^4$s) are not different from the early-time ones, where the majority of the flares can be explained by either internal or external shock. However, due to the small number of flares (a sample of 7 GRBs), the conclusion may require further investigation. Moreover, Bernardini et al. (2011) focused on the late-time flares ($t_{\rm p} \gtrsim 10^3$ s) of a larger sample than Curran et al. (2008) and found that a large fraction of late-time flares are also compatible with afterglow variability. In addition, Lazzati & Perna (2007) showed internal dissipation and external shock mechanisms of X-ray flares, and concluded that at least a sizable fraction of the flares cannot be related to the external shock mechanism, since external shock flares evolve on much longer timescales than observed. Then, some late-time flares in our sample may be related to late-time central engine activity rather than a slower outflow produced simultaneously with the prompt emission. Moreover, the steep decay of X-ray flares is more likely to originate from the internal dissipation (e.g., (Kumar & Panaitescu 2000)). In the present work, we will adopt two criteria to examine the internal or external origin of the flares in our sample, and then study the possible mechanisms for those flares probably related to internal origin.

Several mechanisms and models were proposed to explain the episodic phenomenon of X-ray flares King et al. 2005; Dai et al. 2006; Mészáros 2006; Perna et al. 2006; Lazzati et al. 2008; Lee et al. 2009; Lazzati et al. 2011; Yuan & Zhang 2012; Luo et al. 2013; Hou et al. 2014b. According to the internal origin of X-ray flares, the central engine that powers the prompt gamma-ray emission also powers the X-ray flares. Thus, the long-duration flares require the long-lasting activity of the central engine. For the neutrino annihilation mechanism, as pointed out by Luo et al. (2013), although such a mechanism may work well for the central engine of the gamma-ray emission, it may encounter difficulty in interpreting the X-ray flares. By considering a possible magnetic coupling between the inner disk and the central BH, Luo et al. (2013) showed that the annihilation mechanism can also work for the X-ray flares with duration $\tau \lesssim 100$s. However, the annihilation mechanism is unlikely to be responsible for those long flares with duration $\gtrsim 1000$s, even the role of magnetic coupling is included. On the other hand, according to the analyses of Luo et al. (2013), the BZ mechanism may work well even for the long duration flares. However, outflows were not taken into consideration in Luo et al. (2013), which can be of importance particularly for relatively low accretion rates where the neutrino cooling is inefficient.

There is a positive correlation for the X-ray flares between the duration Δt and the peak time $t_{\rm p}$ (e.g., Margutti et al. 2010; Yi et al. 2016). In the present work, we will focus on the extremely late-time X-ray flares with $t_{\rm p} > 10^4$ s and study the corresponding central engines. The remainder of this paper is organized as follows. Our sample and data analyses are presented in § 2. The different mechanisms for the central engine are investigated in § 3. Conclusions and discussion are made in § 4.

2. SAMPLE AND DATA ANALYSIS

We present an extensive temporal analysis for the X-ray afterglow observed by Swift/XRT, and consider all X-ray afterglow light curves of GRBs detected by Swift/XRT during 11 observation years (from 2005 to 2015) in this repository. The XRT flux lightcurve data and redshift were downloaded from the website `http://www.swift.ac.uk/xrtcurves/` (Evans et al. 2007, 2009). We examined visually all the light curves and searched for bright X-ray flares with extremely late-time, i.e. $F_{\rm p} > 3F$ and $t_{\rm p} > 10^4$s, where $F_{\rm p}$ and F are the peak flux of the flare and the flux of the underlying continuum at $t_{\rm p}$, respectively. We obtain a sample of seven flares from seven GRBs, among

which three GRBs have redshift measurements. The spectral analyses for the steep decay segments are based on http://www.swift.ac.uk/xrtspectra/addspec.php/, which is performed by a power-law spectral model. The spectral analyses results, i.e., the values of the spectral index in the decay phase β, are shown in Table 1.

2.1. *Light-curve fitting*

In order to estimate the duration and luminosity of flares, a smooth broken power-law function (Liang et al. 2007; Li et al. 2012; Yi et al. 2016):

$$F_{\rm t,f} = F_0 \left[(\frac{t}{t_{\rm b}})^{\alpha_1 \omega} + (\frac{t}{t_{\rm b}})^{\alpha_2 \omega} \right]^{-\frac{1}{\omega}} , \tag{1}$$

and a power-law function:

$$F_{\rm t,a} = F_{0,\rm a} t^{-\alpha} , \tag{2}$$

are used to fit the light curves of flares and the underlying continuum, respectively. Here, α_1 (α_2) is the rise (decay) index of X-ray flare, $t_{\rm b}$ is the break time, α is the decay index of the underlying afterglow component, and $\omega = 3$ is used to depict the sharpness around peak flux in the flare light-curve. We would point out that, for the late-time X-ray flares in our sample, it is possible that some of them are a superposition of many shorter flares. In such case, the duration of X-ray flares may be overestimated by a factor of a few. Our main concern in this work is the duration of the flare emission episode. Thus, whether a long-duration flare or many shorter flares may not have essential influence on our analysis.

Each X-ray flare from our sample is fitted by a smooth broken power-law function as shown by Equation (1). The peak time $t_{\rm p}$ can be calculated as

$$t_{\rm p} = t_{\rm b} (-\frac{\alpha_1}{\alpha_2})^{\frac{1}{(\alpha_2 - \alpha_1)\omega}} . \tag{3}$$

The main fitting results are listed in Table 1. As an example, Figure 1 illustrates the fitting procedure of GRB 050502B. Here, we define the duration Δt as the full width at half maximum (FWHM) of the X-ray flares, and

$$\Delta t_{\rm res} = \Delta t / (1+z) \tag{4}$$

is the duration in the rest frame. By setting the zero time T_0 at the GRB trigger time, the flares formed in the external shock process has a maximum decay slope $\alpha_2 = 2 + \beta$, where α_2 and β are the temporal decay index and spectral index in the decay phase, respectively. Any decay with a slope steeper than $2 + \beta$, i.e. $\alpha_2 > 2 + \beta$, may indicate the internal origin of flares (Kumar & Panaitescu 2000; Liang et al. 2006). Then, we compare the values of α_2 and $2 + \beta$ for our seven late-time X-ray flares in Figure 2. It is seen that four flares in our sample locate well above the red solid line, which means that the four flares satisfy the criterion "$\alpha_2 > 2 + \beta$", and therefore are likely to be internal origin. In the remainder, we will focus on these four flares.

2.2. *Isotropic luminosity and energy*

The isotropic energy $E_{\rm X,iso}$ of a single X-ray flare in XRT energy range is calculated by

$$E_{\rm X,iso} = \frac{4\pi D_{\rm L}^2 S_{\rm F}}{1+z} , \tag{5}$$

where $D_{\rm L}$ is the distance of GRB with respect to the observer, and

$$S_{\rm F} = \int_{0.1t_1}^{10t_2} F_0 \left[(\frac{t}{t_{\rm b}})^{\alpha_1 \omega} + (\frac{t}{t_{\rm b}})^{\alpha_2 \omega} \right]^{-\frac{1}{\omega}} dt , \tag{6}$$

is the energy fluence in the energy range of Swift/XRT (i.e., 0.3-10 keV). Here, t_1 and t_2 ($t_1 < t_2$) can be derived by the two cross points of the two curves corresponding to Equations (1) and (2) (see Falcone et al. (2007) and Yi et al. (2016)). We choose a sufficiently large time interval, i.e., from $0.1t_1$ to $10t_2$, for the integration of Equation (1). The isotropic luminosity $L_{\rm X,iso}$ of a single X-ray flare is expressed as

$$L_{\rm X,iso} = \frac{(1+z) E_{\rm X,iso}}{\Delta t} . \tag{7}$$

In addition, the anisotropic effects of the jet radiation should be taken into account. We adopt $1 - \cos\theta_{\rm jet} \approx 0.1$, i.e., $\theta_{\rm jet} \sim 0.45$ radian, where $\theta_{\rm jet}$ is the half-opening angle of the jet related to the flares. This value is around one order of magnitude larger than the prompt gamma-ray emission (~ 0.05 radian) (Zeh et al. 2006). The reason of

adopting such a value is that there may exist a relation $\gamma\theta_{\rm jet} \sim 20$ (Tchekhovskoy et al. 2010b), and the Lorentz factor γ of the jet producing the X-ray flares may be significantly smaller than that of the gamma-ray emission. Thus, the collimated-corrected energy $E_{\rm X} = E_{\rm X,iso}(1-\cos\theta_{\rm jet}) = 0.1E_{\rm X,iso}$ and luminosity $L_{\rm X} = 0.1L_{\rm X,iso}$. The main results are shown in Table 2, where the uncertainties of luminosity and energy are given at 1 σ. More details about the uncertainties may refer to Yi et al. (2016). We would point out that the k-correction is not considered in the present work. The luminosity and energy will be higher if the k-correction is taken into account. Here, we adopt $z = 2$ for those flares without redshift measurements (Salvaterra et al. 2012). In order to explore the range of variability of the luminosity and energy for all possible values of the unknown redshift, we use $z = 0.1$ and 10 as the lower and upper limits, respectively.

With the above results, we can examine the relationship between the relative variability flux $\Delta F/F$ and the relative variability timescale $\Delta t/t_{\rm p}$, where ΔF is the increase of flux at the peak time $t_{\rm p}$, and F is the flux of the underlying continuum at $t_{\rm p}$ (see Ioka et al. (2005) and Bernardini et al. (2011) for details). In Figure 3, we plot exactly the same five theoretical solid lines as those in Figure 6 of Bernardini et al. (2011). The data for our seven late-time X-ray flares are also plotted by different colors in this figure. Another criterion to judge the internal origin or not is to examine the position of a flare in such a figure. A flare locating in the upper left region (above the green line and left to the vertical pink line) can be regarded as the internal origin. On the contrary, the flare locating in other regions may be related to the external origin. It is seen that two flares (050916 and 130925A) well locate in the upper left region, which corresponds to the internal origin. On the other hand, the other five flares do not locate in this region, which indicates that the five flares may be related to the external origin. By combining the results of Figures 2 and 3, we can draw the conclusion that, the late-time flares of 050916 and 130925A are probably related to the late-time activity of central engine since both of the two criteria are satisfied, whereas the flares of 070318, 070429A, and 150626B are more likely to be the external origin since neither of the two criteria is matched. For the rest two flares 050502B and 050724, however, the physical origin may remain controversial since the criterion "$\alpha_2 > 2+\beta$" is matched but the other one is not. In particular, for the only short burst 050724, we noticed that some previous works suggested late-time activity of central engine (Fan et al. 2005; Dai et al. 2006), while some other works such as Bernardini et al. (2011) argued against internal origin.

In the rest part of this paper, we will focus on the four X-ray flares which can satisfy at least one criterion, i.e., 050502B, 050724, 050916, and 130925A. The main purpose is to investigate the possible central engine, where the internal origin is our basic assumption for such flares.

3. MECHANISMS OF THE CENTRAL ENGINE

In this section, we focus on the central engine of the sample of the four late-time X-ray flares based on the energy argument. As mentioned in Section 1, there are two well-known mechanisms related to accreting BHs, i.e., the neutrino-antineutrino annihilation and the BZ process. We study these two mechanisms in the first and second subsections, respectively. In addition, we discuss the possibility of an NS system as the engine in the third subsection.

3.1. *Neutrino-antineutrino annihilation*

In this subsection, we calculate the neutrino annihilation luminosity based on previous theoretical formulae. We assume a typical BH mass $M_{\rm BH} = 3M_\odot$ and a spin parameter $a_* = 0.95$. We adopt the analytic result, Equation (22) of Zalamea & Beloborodov (2011) to calculate the annihilation luminosity:

$$L_{\nu\bar{\nu}} \approx 1.1\times10^{52}\chi_{\rm ms}^{-4.8}\left(\frac{M_{\rm BH}}{3M_\odot}\right)^{-3/2}\times\left\{\begin{array}{ll} 0 & \frac{M_{\rm sup}}{\Delta t} < \dot{M}_{\rm ign} \\ \left(\frac{M_{\rm sup}/\Delta t}{M_\odot {\rm s}^{-1}}\right)^{9/4} & \dot{M}_{\rm ign} < \frac{M_{\rm sup}}{\Delta t} < \dot{M}_{\rm trap} \\ \left(\frac{\dot{M}_{\rm trap}}{M_\odot {\rm s}^{-1}}\right)^{9/4} & \frac{M_{\rm sup}}{\Delta t} > \dot{M}_{\rm trap} \end{array}\right\} {\rm erg\ s^{-1}}\ , \quad (8)$$

where $\chi_{\rm ms} = r_{\rm ms}(a_*)/r_{\rm g}$, $r_{\rm g} \equiv 2GM_{\rm BH}/c^2$, $r_{\rm ms}$ is the radius of the marginally stable orbit.

Following the spirit of Rowlinson et al. (2014), we assume an efficiency η as the ratio of the radiated luminosity to the jet power, where the latter may be regarded as around $L_{\nu\bar{\nu}}$,

$$L_{\rm X} = \eta\ L_{\nu\bar{\nu}}\ . \quad (9)$$

Here, we adopt $\eta = 10\%$ for analyses. The analytic solution about $r_{\rm ms}$ (Bardeen et al. 1972) gives $r_{\rm ms} = 0.97r_{\rm g}$ for $a_* = 0.95$, i.e., $\chi_{\rm ms} = r_{\rm ms}(a_*)/r_{\rm g} = 0.97$. The two critical accretion rates, $\dot{M}_{\rm ign}$ and $\dot{M}_{\rm trap}$, were given by

Equation (5) of Zalamea & Beloborodov (2011). We adopt $\alpha = 0.1$ as Zalamea & Beloborodov (2011) and therefore $\dot{M}_{\rm ign} \approx 0.021 M_\odot$ s^{-1} and $\dot{M}_{\rm trap} \approx 1.8 M_\odot$ s^{-1}.

For the neutrino annihilation mechanism, a comparison between the theoretical results and the observations is shown in Figure 4. For the observations, following the argument in Section 2.2, we adopt $L_{\rm X} = 0.1 L_{\rm X,iso}$ with regard to the anisotropic effects. The red solid lines represent our analytic results for the supplied mass $M_{\rm sup} = 0.1 M_\odot$ and $M_\odot$. Since $M_{\rm sup}$ is the mass supply after the prompt emission, one $M_\odot$ may be regarded as an upper limit for $M_{\rm sup}$. For a fixed $M_{\rm sup}$, if outflows are not considered, once the duration $\Delta t_{\rm res}$ is given, the mean mass accretion rate can be estimated as $\dot{M} = M_{\rm sup}/\Delta t_{\rm res}$. Then, by Equation (8), we can derive the theoretical annihilation luminosity. The gray stars in Figure 4 represent the observational results for X-ray flares with $\Delta t_{\rm res} < 100$ s, which are taken from Luo et al. (2013). The blue and green circles represent the two late-time flares with redshift measurement, whereas the magenta and orange circles represent the other two flares without redshift measurement, where $z = 2$ is adopted. The lower limit ($z = 0.1$) and the upper limit ($z = 10$) are also shown by the arrows in the same colors. As shown in Figure 4, the annihilation mechanism can account for only a small fraction of X-ray flares with $\Delta t_{\rm res} < 100$ s. As proposed in Luo et al. (2013), if the magnetic coupling effects between the inner disk and the central BH are included, the annihilation mechanism may work for $\Delta t_{\rm res} < 100$ s, but still encounter difficulty in interpreting the flares with $\Delta t_{\rm res} \gtrsim 1000$ s. It is seen from Figure 4 that, even for $M_{\rm sup} = M_\odot$ the theoretical red line is far from the color circles, which reveals that the annihilation luminosity is too low to power such late-time X-ray flares. In addition, other analytic formulae were proposed for the annihilation luminosity, such as Equation (11) of Fryer et al. (1999) and Equation (1) of Liu et al. (2016). These two analytic formulae can confirm the above conclusion that the annihilation mechanism cannot work as the central engine for the extremely late-time flares with $t_{\rm p} > 10^4$ s.

3.2. *Blandford-Znajek process*

An alternative mechanism related to BHs for the central engine for GRBs and corresponding X-ray flares is the well-known BZ process (Blandford & Znajek 1977), where the rotational energy of BHs can be extracted by the strong magnetic fields and therefore power a relativistic jet. Following Popham et al. (1999) and Di Matteo et al. (2002), based on a common assumption that the magnetic field B is around 10% of its equipartition value, the analytic BZ jet power can be expressed as

$$P_{\rm BZ} \approx 10^{51} a_*^2 \left(\frac{M_{\rm BH}}{3M_\odot}\right)^2 \left(\frac{\dot{M}_{\rm in}}{M_\odot \ {\rm s}^{-1}}\right) \ {\rm erg \ s^{-1}} \ , \tag{10}$$

where $\dot{M}_{\rm in}$ is the mass accretion rate near the BH horizon. Similar to the neutrino annihilation case, we use η to describe the ratio of the radiated luminosity to the power,

$$L_{\rm BZ} = \eta \ P_{\rm BZ} \ , \tag{11}$$

where $\eta = 10\%$ is adopted. For the case of extremely late-time X-ray flares with duration $\gtrsim 10^4$s, the mean supplied mass accretion rate ought to be relatively low $\dot{M}_{\rm sup} \lesssim M_{\rm sup}/\tau_{\rm res} \lesssim 10^{-4} M_\odot$ s^{-1}. In such case, the neutrino cooling will be negligible compared with the viscous heating. In this scenario, outflows ought to be quite strong (see the discussions in Section 4) such that $\dot{M}_{\rm in}$ will be significantly less than $\dot{M}_{\rm sup}$. Following previous works on outflows, we take the radial profile of the net inflow accretion rate as

$$\dot{M}_{\rm in} = \dot{M}_{\rm out} \left(\frac{r_{\rm in}}{r_{\rm out}}\right)^p \ , \tag{12}$$

where $p \approx 1$ according to the analyses and simulations of super-Eddington accretion flows (Ohsuga et al. 2005; Gu 2012), and $\dot{M}_{\rm out}$ may be roughly evaluated as $\approx \dot{M}_{\rm sup}$. We assume $r_{\rm out}/r_{\rm in} \gtrsim 100$ according to the hyper-accretion case. Then, Equation (12) gives $\dot{M}_{\rm in}/\dot{M}_{\rm out} \lesssim 1\%$. In other words, more than 99% of the supplied mass will not enter the BH, but escape from the disk by outflows. It is obvious from Equation (10) that such outflows will have essential influence on the power of the BZ process. By combining Equations (10)-(12) we can derive the following relationship:

$$L_{\rm X} \approx 10^{48} a_*^2 \left(\frac{M_{\rm sup}/\Delta t_{\rm res}}{M_\odot \ {\rm s}^{-1}}\right) \ {\rm erg \ s^{-1}} \ . \tag{13}$$

In order to directly compare the theory and the observation, the anisotropic effects of jet radiation should be considered. The relation between the BZ luminosity and the isotropic luminosity takes the form,

$$L_{\rm BZ} = L_{\rm X,iso} \ (1 - \cos\theta_{\rm jet}) \ , \tag{14}$$

where $1-\cos\theta_{\rm jet}\approx 0.1$ is adopted as discussed in Section 2.2.

A comparison of the theoretical results with the observations is shown in Figure 5. The two pairs of solid lines correspond to our theoretical results for $a_*=0.8$ (green) and 0.95 (red), which are calculated by Equation (13). For the two lines in the same color, the upper line corresponds to $M_{\rm sup}=M_\odot$, and the lower line corresponds to $M_{\rm sup}=0.1M_\odot$. Similar to Figure 4, the blue and green circles represent the observed X-ray flares with redshift measurements. The magenta and orange circles represent the other two flares without redshift measurement, where $z=2$ is adopted. The lower limit ($z=0.1$) and the upper limit ($z=10$) are also shown by the arrows in the same colors. It is seen from Figure 5 that, even for the extreme case with $M_{\rm sup}=M_\odot$ and $a_*=0.95$, the BZ mechanism can hardly account for these four flares. The physical reason is that, due to the strong outflows, the mass rate near the BH horizon is quite low (generally $\lesssim 10^{-6}M_\odot$ s^{-1}), and therefore the magnetic fields accumulated by the accretion will probably be too weak to power such flares. Thus, for the extreme late-time X-ray flares, the BZ mechanism may not work as the central engine either.

As shown by Equation (10), we adopt $L_{\rm BZ}\propto a_*^2$ for the analyses, which agrees with the simulation results on geometrically thin disks (Tchekhovskoy et al. 2010a). On the other hand, Tchekhovskoy et al. (2010a) showed that, for geometrically thick disks, however, the relation will be $L_{\rm BZ}\propto a_*^4$ or even $\propto a_*^6$ for fast rotating cases ($a_*\to 1$). In other words, the jet luminosity $L_{\rm BZ}$ will decrease sharply with decreasing a_* (e.g., Figure 6 of Tchekhovskoy et al. 2010a). For the flow with relatively low accretion rates $\lesssim 10^{-4}M_\odot$ s^{-1}, the neutrino cooling will be inefficient and therefore the disk is likely to be geometrically thick (Gu 2015). As a consequence, our analytic $L_{\rm BZ}$ for $a_*<1$ may be overestimated and therefore $L_{\rm BZ}$ in the real cases may be even lower such that it may not be responsible for the late-time flares.

3.3. *Neutron star with strong bipolar magnetic fields*

The above two subsections have shown that the central engine for the extremely late-time X-ray flares is unlikely to be associated with BHs. In this subsection, we study the possibility of an NS system as the engine. Such a model invokes a rapidly spinning, strongly magnetized NS or a magnetar (Usov 1992; Thompson 1994; Dai & Lu 1998; Wheeler et al. 2000; Zhang & Mészáros 2001; Metzger et al. 2008, 2011; Bucciantini et al. 2012). In the NS scenario, the energy reservoir is the total rotational energy of the magnetized NS, (see Equation (1) in Lü & Zhang (2014)):

$$E_{\rm rot}\approx 2\times 10^{52}\frac{M_{\rm NS}}{1.4M_\odot}\left(\frac{R}{10^6{\rm cm}}\right)^2\left(\frac{P_0}{10^{-3}{\rm s}}\right)^{-2}\ {\rm erg}\ , \tag{15}$$

where $M_{\rm NS}$ is the NS mass and P_0 is the initial spin period. We therefore take $E_{\rm rot}=2\times 10^{52}$erg as a typical rotational energy. Another energy source is the magnetic energy of a magnetar. The total magnetic energy in a magnetar can be roughly calculated by

$$E_{\rm mag}\approx\frac{B^2}{8\pi}\times\frac{4}{3}\pi R^3=\frac{1}{6}B^2R^3\ , \tag{16}$$

where B is the poloidal magnetic field strength on the horizon. With $R\approx 10^6$cm, the total magnetic energy is $E_{\rm mag}=1.7\times 10^{47}$erg for $B=10^{15}$G.

A comparison of the rotational energy and the magnetic energy with the observations of the X-ray flares is shown in Figure 6. Again, we choose $1-\cos\theta_{\rm jet}=0.1$ due to the anisotropic effects, and the radiative efficiency $\eta=10\%$. For a GRB with multiple flares, we plot the total energy of all the flares instead of the single late-time flare. It is seen that, the energy of flares is significantly larger than the magnetic energy even for $B=10^{15}$G, which implies that the magnetic energy may not power the X-ray flares. Or, the magnetic energy can only work with extremely strong magnetic fields $B\gg 10^{15}$G. Such an issue has been investigated by Dai et al. (2006). On the other hand, the rotational energy (red dashed line) is obviously higher than all the observational data, which indicates that the rotational energy may be responsible for the late-time X-ray flares in our sample.

4. CONCLUSIONS AND DISCUSSION

The present work focuses on the central engine of extremely late-time X-ray flares ($t_{\rm p}>10^4$s) with the internal origin assumption. We have investigated the possibility of the two well-known mechanisms related to BHs for the central engine, i.e., the neutrino-antineutrino annihilation and the BZ process. Our results show that the annihilation luminosity is far below the observational data, which indicates that the annihilation mechanism cannot account for the extremely late-time X-ray flares. On the other hand, for the BZ process, if the role of outflows is taken into consideration, the inflow mass rate near the horizon will be quite low such that the magnetic field will probably be too

weak to power the observed X-ray flares. We therefore argue that, for such late-time X-ray flares, the central engine is unlikely to be associated with BHs. On the contrary, a fast rotating NS with strong bipolar magnetic fields may be responsible for such flares. We would stress that this work only considered bright flares. Some dim flares at late-time may be missed since the underlying continuum is too bright for their detection. These dim flares may occupy the lower part of Figures 5 and 6, which are possibly consistent with the BZ mechanism and the magnetic origin in the magnetar context (Margutti et al. 2011).

In this work, the existence of outflows is a key point to draw the conclusion that the BZ mechanism is unlikely to power the extremely late-time X-ray flares. In recent years, outflows have been found to be significant in accretion systems of different scales by theories (e.g., Jiao & Wu 2011; Gu 2015), simulations (e.g., Ohsuga et al. 2005; Ohsuga & Mineshige 2011; Yuan et al. 2012a,b; Jiang et al. 2014; Sądowski & Narayan 2015, 2016), and observations (e.g., Wang et al. 2013). Based on the balance of heating and cooling, Gu (2015) shows that the outflow is inevitable for the accretion flows that the radiative cooling is far below the viscous heating, no matter the flow is optically thin or thick. In the current work for accretion rates $\dot{M} \lesssim 10^{-4} M_{\odot} \mathrm{s}^{-1}$, neither the photon radiative cooling nor the neutrino one is efficient to balance the viscous heating. Thus, the outflows ought to be significant. Actually, Liu et al. (2008) studied this issue and proposed that there exists a lower critical $\dot{M}$ varying with radius, below which outflows have to occur. From the observational view, taking our Galactic center as an example, Wang et al. (2013) reveals that more than 99% of the accreted mass escape from the accretion flow by outflows. Therefore, it is reasonable to assume less than 1% of the supplied mass can enter the BH in the present work.

The present work focuses on the late-time X-ray flares with $t_{\rm p} > 10^4$s. On the other hand, a previous work (Luo et al. 2013) focused on the X-ray flares with rest duration $\Delta t \lesssim 100$s, and found that the neutrino annihilation mechanism cannot account for the flares except for including the magnetic coupling between the inner disk and the BH. However, such a coupling and corresponding distribution of magnetic fields have not been found in simulations yet. Thus, we would argue that, in general, the annihilation mechanism may not work as the central engine for X-ray flares. For the BZ mechanism, the output power is larger than that of the annihilation mechanism, particularly for relatively low accretion rates. From the energy argument, the BZ mechanism may be responsible for X-ray flares with duration $\Delta t_{\rm res} \lesssim 10^4$ s in the case that outflows are not significant.

We acknowledge the use of the public data from the Swift data archive. We thank Xue-Feng Wu, Hao Tong, Bing Zhang, and Jirong Mao for beneficial discussions, and thank the referee for constructive suggestions that improved the paper. This work was supported by the National Basic Research Program of China (973 Program) under grants 2014CB845800, the National Natural Science Foundation of China under grants 11573023, 11533003, 11503011, 11473022, 11403005, 11333004, 11233006, 11222328, and U1331101, the CAS Open Research Program of Key Laboratory for the Structure and Evolution of Celestial Objects under grant OP201503, and the Fundamental Research Funds for the Central Universities under grants 20720140532 and 20720160024.

REFERENCES

Bardeen, J. M., Press, W. H., & Teukolsky, S. A. 1972, ApJ, 178, 347
Bernardini, M. G., Margutti, R., Chincarini, G., Guidorzi, C., & Mao, J. 2011, A&A, 526, A27
Birkl, R., Aloy, M. A., Janka, H.-T., Müller, E. 2007, A&A, 463, 51
Blandford, R. D., & Znajek, R. L. 1977, MNRAS, 179, 433
Bucciantini, N., Metzger, B. D., Thompson, T. A., & Quataert, E. 2012, MNRAS, 419, 1537
Burrows, D. N., Hill,J. E., Nousek, J. A., et al. 2005a, SSRv, 120, 165
Burrows, D. N., Romano, P., Falcone, A., et al. 2005b, Science, 309, 1833
Campana, S., Tagliaferri, G., Lazzati, D., et al. 2006, A&A, 454, 113
Cao, X., Liang, E.-W., & Yuan, Y.-F. 2014, ApJ, 789, 129
Chincarini, G., Mao, J., Margutti, R., et al. 2010, MNRAS, 406, 2113
Chincarini, G., Moretti, A., Romano, P., et al. 2007, ApJ, 671, 1903
Curran, P. A., Starling, R. L. C., O'Brien, P. T., et al. 2008, A&A, 487, 533
Dai, Z. G., & Lu, T. 1998, A&A, 333, L87
Dai, Z. G., Wang, X. Y.,Wu, X. F., & Zhang, B. 2006, Science, 311, 1127
Di Matteo, T., Perna, R., & Narayan, R. 2002, ApJ, 579, 706
Evans, P. A., Beardmore, A. P., Page, K. L., et al. 2009, MNRAS, 397, 1177
Evans, P. A., Beardmore, A. P., Page, K. L., et al. 2007, A&A, 469, 379
Falcone, A. D., Burrows, D. N., Lazzati, D., et al. 2006, ApJ, 641, 1010
Falcone, A. D., Morris, D., Racusin, J., et al. 2007, ApJ, 671, 1921
Fan, Y. Z., Zhang, B., & Proga, D. 2005, ApJL, 635, L129
Fryer, C. L., Woosley, S. E., Herant, M., & Davies, M. B. 1999, ApJ, 520, 650
Grupe, D. 2006, XMM-Newton Proposal, 05025202
Gu, W.-M., Liu, T., & Lu, J.-F. 2006, ApJL, 643, L87
Gu, W.-M. 2012, ApJ, 753, 118

Gu, W.-M. 2015, ApJ, 799, 71
Hou, S. J., Geng, J. J., Wang, K., et al. 2014a, ApJ, 785, 113
Hou, S.-J., Liu, T., Gu, W.-M., et al. 2014b, ApJL, 781, L19
Ioka, K., Kobayashi, S., & Zhang, B. 2005, ApJ, 631, 429
Janiuk, A., Mioduszewski, P., & Moscibrodzka, M. 2013, ApJ, 776, 105
Jiang, Y.-F., Stone, J. M., & Davis, S. W. 2014, ApJ, 796, 106
Jiao, C.-L., & Wu, X.-B. 2011, ApJ, 733, 112
Kawanaka, N., & Mineshige, S. 2007, ApJ, 662, 1156
King, A., O'Brien, P. T., Goad, M. R., et al. 2005, ApJL, 630, L113
Kumar, P., & Panaitescu, A. 2000, ApJL, 541, L51
Lü, H.-J., & Zhang, B. 2014, ApJ, 785, 74
Lazzati, D., Blackwell, C. H., Morsony, B. J., & Begelman, M. C. 2011, MNRAS, 411, L16
Lazzati, D., & Perna, R. 2007, MNRAS, 375, L46
Lazzati, D., Perna, R., & Begelman, M. C. 2008, MNRAS, 388, L15
Lee, W. H., Ramirez-Ruiz, E., & López-Cámara, D. 2009, ApJL, 699, L93
Lei, W. H., Wang, D. X., Zhang, L., et al. 2009, ApJ, 700, 1970
Li, L., Liang, E.-W., Tang, Q.-W., et al. 2012, ApJ, 758, 27
Liang, E.-W., Yi, S.-X., Zhang, J., et al. 2010, ApJ, 725, 2209
Liang, E. W., Zhang, B., O'Brien, P. T., et al. 2006, ApJ, 646, 351
Liang, E.-W., Zhang, B.-B., & Zhang, B. 2007, ApJ, 670, 565
Liu, T., Gu, W.-M., Xue, L., & Lu, J.-F. 2007, ApJ, 661, 1025
Liu, T., Gu, W.-M., Xue, L., Weng, S.-S., & Lu, J.-F. 2008, ApJ, 676, 545
Liu, T., Xue, L., Gu, W.-M., & Lu, J.-F. 2013, ApJ, 762, 102
Liu, T., Xue, L., Zhao, X.-H., Zhang, F.-W., & Zhang, B. 2016,ApJ, 821, 132
Liu, T., Yu, X.-F., Gu, W.-M., & Lu, J.-F. 2014, ApJ, 791, 69
Luo, Y., Gu, W.-M., Liu, T., & Lu, J.-F. 2013, ApJ, 773, 142
Mészáros, P. 2006, Reports on Progress in Physics, 69, 2259
Margutti, R., Bernardini, G., Barniol Duran, R., et al. 2011,MNRAS, 410, 1064
Margutti, R., Guidorzi, C., Chincarini, G., et al. 2010, MNRAS, 406, 2149
Metzger, B. D., Giannios, D., Thompson, T. A., Bucciantini, N.,& Quataert, E. 2011, MNRAS, 413, 2031
Metzger, B. D., Quataert, E., & Thompson, T. A. 2008, MNRAS, 385, 1455
Nousek, J. A., Kouveliotou, C., Grupe, D., et al. 2006, ApJ, 642, 389
O'Brien, P. T., Willingale, R., Osborne, J., et al. 2006, ApJ, 647, 1213
Ohsuga, K., & Mineshige, S. 2011, ApJ, 736, 2
Ohsuga, K., Mori, M., Nakamoto, T., & Mineshige, S. 2005, ApJ, 628, 368
Pan, Z., & Yuan, Y.-F. 2012, ApJ, 759, 82
Perna, R., Armitage, P. J., & Zhang, B. 2006, ApJL, 636, L29
Popham, R., Woosley, S. E., & Fryer, C. 1999, ApJ, 518, 356
Romano, P., Moretti, A., Banat, P. L., et al. 2006, A&A, 450, 59
Rowlinson, A., Gompertz, B. P., Dainotti, M., et al. 2014, MNRAS, 443, 1779
Sądowski, A., & Narayan, R. 2015, MNRAS, 453, 3213
Sądowski, A., & Narayan, R. 2016, MNRAS, 456, 3929
Salvaterra, R., Campana, S., Vergani, S. D., et al. 2012, ApJ, 749, 68
Tchekhovskoy, A., Narayan, R., & McKinney, J. C. 2010a, ApJ, 711, 50
Tchekhovskoy, A., Narayan, R., & McKinney, J. C. 2010b, NewA, 15, 749
Thompson, C. 1994, MNRAS, 270, 480
Usov, V. V. 1992, Nature, 357, 472
Wang, Q. D., Nowak, M. A., Markoff, S. B., et al. 2013, Science, 341, 981
Wheeler, J. C., Yi, I., Höflich, P., & Wang, L. 2000, ApJ, 537, 810
Wu, X.-F., Hou, S.-J., & Lei, W.-H. 2013, ApJL, 767, L36
Xue, L., Liu, T., Gu, W.-M., & Lu, J.-F. 2013, ApJS, 207, 23
Yi, S.-X., Wu, X.-F., Wang, F.-Y., & Dai, Z.-G. 2015, ApJ, 807, 92
Yi, S.-X., Xi, S.-Q., Yu, H., et al. 2016, ApJS, 224, 20
Yuan, F., Bu, D., & Wu, M. 2012a, ApJ, 761, 130
Yuan, F., Wu, M., & Bu, D. 2012b, ApJ, 761, 129
Yuan, F., & Zhang, B. 2012, ApJ, 757, 56
Zalamea, I., & Beloborodov, A. M. 2011, MNRAS, 410, 2302
Zeh, A., Klose, S., & Kann, D. A. 2006, ApJ, 637, 889
Zhang, B. 2011, Comptes Rendus Physique, 12, 206
Zhang, B., Fan, Y. Z., Dyks, J., et al. 2006, ApJ, 642, 354
Zhang, B., & Mészáros, P. 2001, ApJL, 552, L35
Zhang, B., Liang, E., Page, K. L., et al. 2007, ApJ, 655, 989

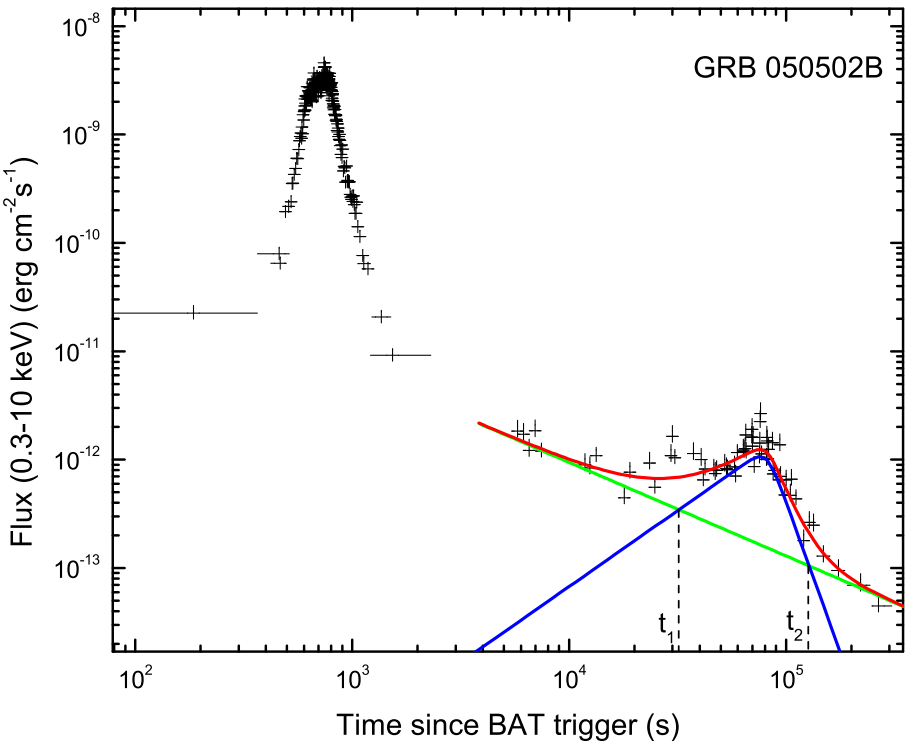

Figure 1. The best fitting for the late-time X-ray afterglow light curve of GRB 050502B (red curve). The blue curve and the green line show the best fitting of the late-time flare and the underlying continuum, respectively. The first flare is not considered in this fitting.

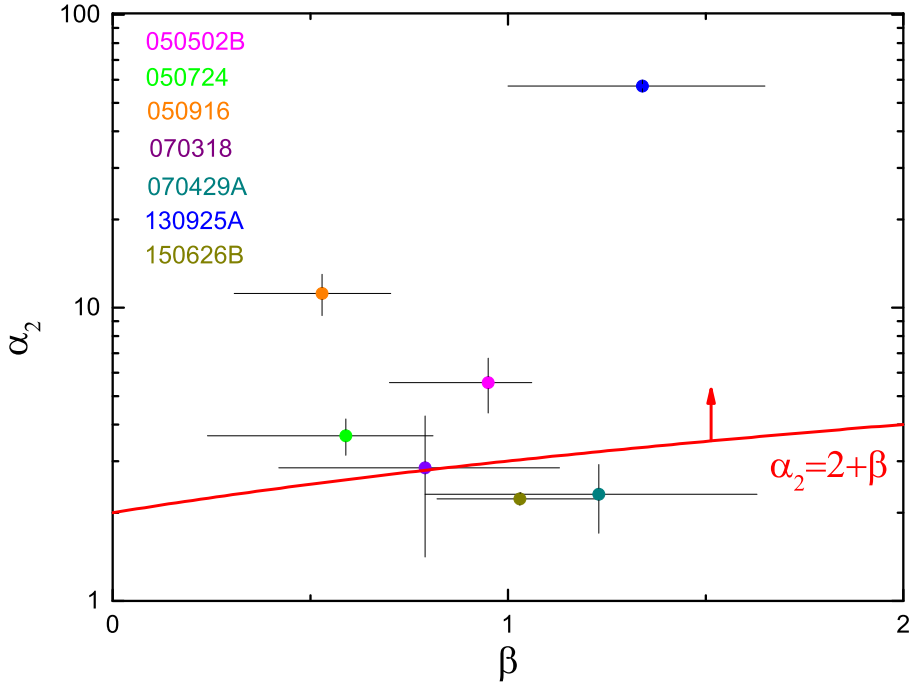

Figure 2. A comparison of the seven late-time flares in our sample with the criterion of internal origin "$\alpha_2 > 2 + \beta$".

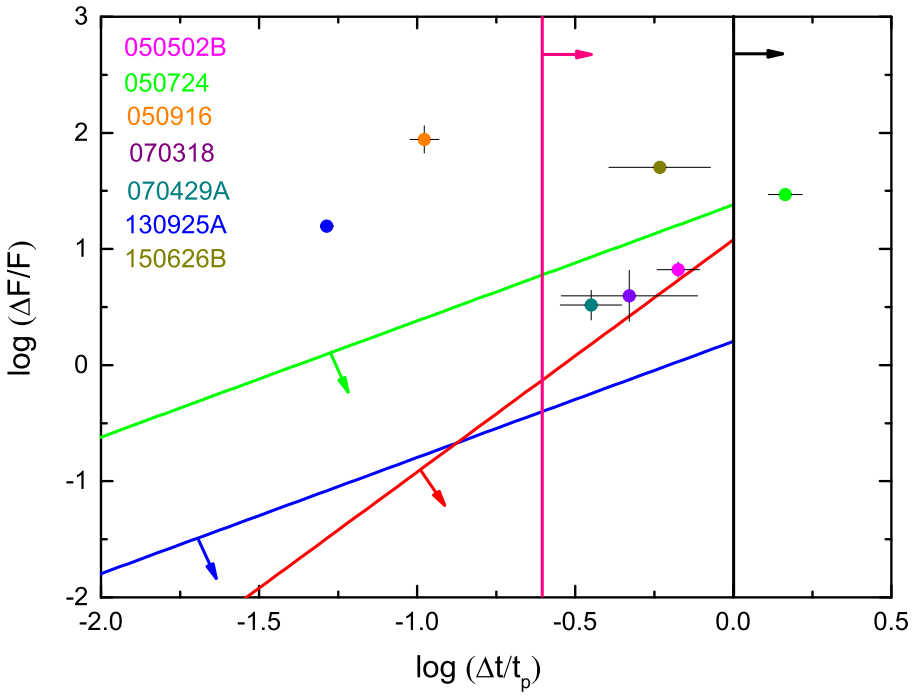

Figure 3. The relationship between the relative variability flux $\Delta F/F$ and the relative variability timescale $\Delta t/t_{\rm p}$ for the seven late-time X-ray flares in our sample. The five theoretical solid lines are identical with those in Figure 6 of Bernardini et al. (2011), i.e., density fluctuations on axis (blue line) and off-axis (red line), off-axis multiple regions density fluctuations (green line), patchy shell model (black line), and refreshed shocks (pink line).

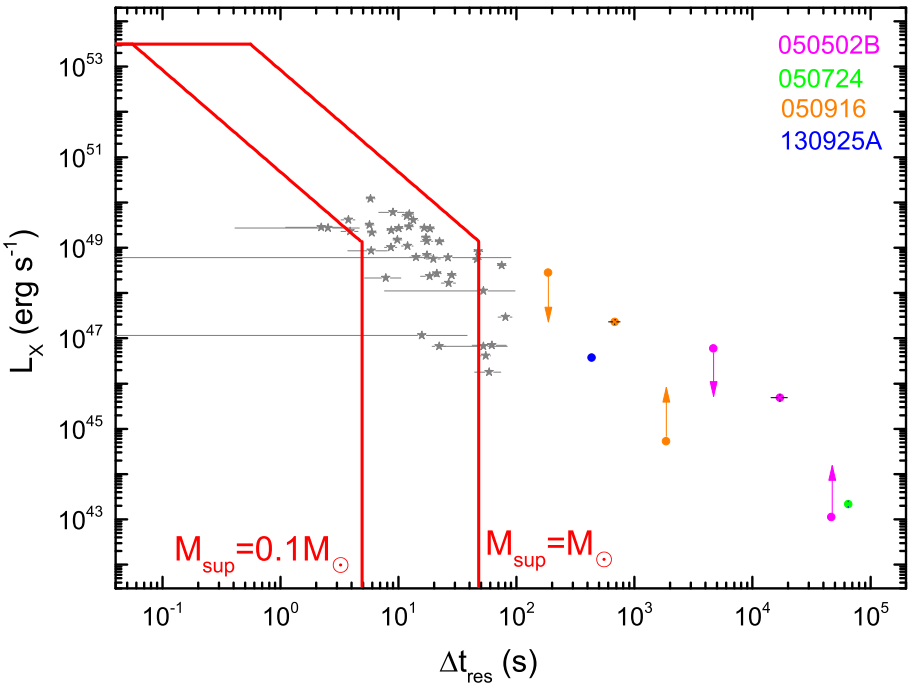

Figure 4. Comparison of the theoretical results (red solid lines) with the observations (symbols) in the $L_{\rm X} - \Delta t_{\rm res}$ diagram for the neutrino annihilation mechanism. The theoretical annihilation luminosity is calculated by Equation (8). The left and right red lines correspond to the supplied mass $M_{\rm sup} = 0.1 M_\odot$ and $M_\odot$, respectively. The gray stars are taken from Luo et al. (2013) corresponding to flares with $\Delta t_{\rm res} < 100$s. The blue and green circles represent the two late-time flares with redshift measurement, whereas the magenta and orange circles represent the other two flares without redshift measurement, where $z = 2$ is adopted. The lower limit ($z = 0.1$) and the upper limit ($z = 10$) are also shown by the arrows in the same colors.

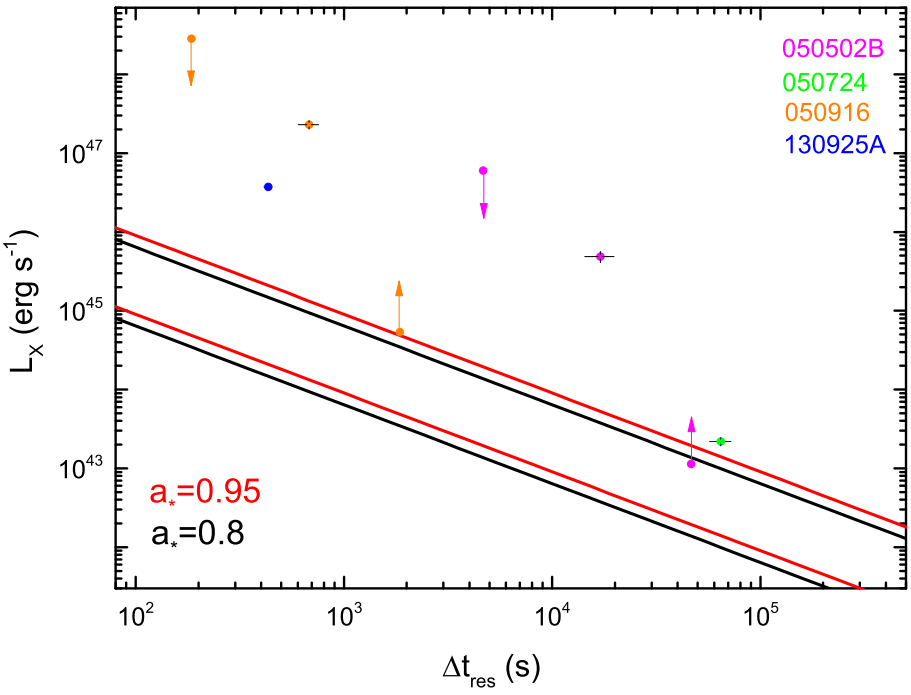

Figure 5. Comparison of the theoretical results of the BZ mechanism with the observations, where two typical values for the spin parameters $a_* = 0.8$ (black) and 0.95 (red) are fixed. For the two lines in the same color, the upper line corresponds to $M_{\rm sup} = M_\odot$, and the lower line corresponds to $M_{\rm sup} = 0.1\ M_\odot$. The meaning of the circles and arrows is the same as in Figure 4.

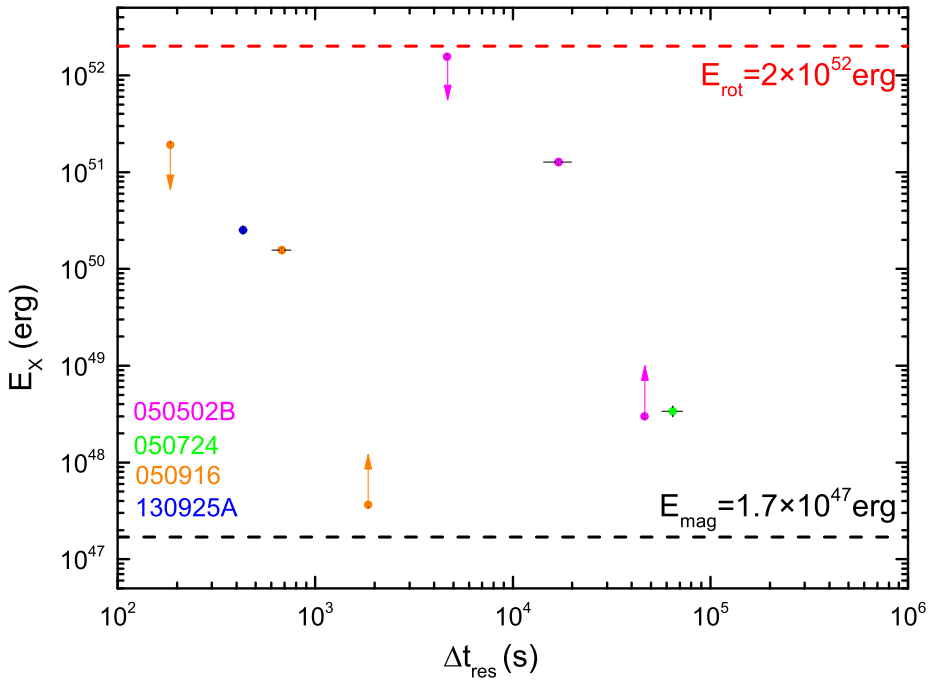

Figure 6. Energy of the X-ray flares in our sample. For a GRB with multiple flares, the total energy of all the flares is plotted. The red dashed line represents the energy related to the rotational energy of a fast rotating NS, and the black dashed line corresponds to the energy related to the magnetic energy of a magnetar with $B = 10^{15}$G. The meaning of the four colors is the same as in Figure 4.

Table 1. Fitting results of the late-time flares.

GRB	z	α_1	α_2	$t_1 - t_2$ (10^4 s)	$t_{\rm p}$ (10^4 s)	$F_{\rm p}$ (erg cm^{-2}s^{-1})	β	χ^2/dof
050502B	–	-1.40 ± 0.41	5.56 ± 1.18	3.22 - 12.82	7.63 ± 0.38	(1.08 ± 0.15)× 10^{-12}	$0.95^{+0.25}_{-0.11}$	2.33
050724	0.257	-2.04 ± 0.44	3.66 ± 0.52	1.72 - 22.09	5.56 ± 0.31	(1.90 ± 0.22)× 10^{-12}	$0.59^{+0.35}_{-0.22}$	1.32
050916	–	-33.68 ± 3.10	11.20 ± 1.80	1.68 - 3.06	1.93 ± 0.02	(3.76 ± 1.15)× 10^{-11}	$0.53^{+0.22}_{-0.17}$	1.27
130925A	0.347	-24.49 ± 2.01	57.02 ± 1.11	1.01 - 1.19	1.12 ± 0.01	(6.18 ± 0.19)× 10^{-10}	$1.34^{+0.34}_{-0.31}$	1.62
070318	0.84	-1.52 ± 1.28	2.84 ± 1.43	14.03 - 37.21	19.46 ± 3.02	(3.35 ± 1.08)× 10^{-13}	$0.79^{+0.37}_{-0.34}$	1.53
070429A	–	-11.54 ± 11.72	2.31 ± 0.61	21.23 - 90.79	23.44 ± 1.43	(2.13 ± 0.05)× 10^{-13}	$1.23^{+0.44}_{-0.40}$	1.15
150626B	–	-1.08 ± 0.12	2.23 ± 0.11	0.33 - 114.37	2.11 ± 0.08	(1.08 ± 0.05)× 10^{-13}	$1.03^{+0.21}_{-0.20}$	0.86

Table 2. Physical parameters based on the fitting results

GRB	Δt (s)	$\Delta F/F$	$E_{\rm X}$ (erg)	$L_{\rm X}$ (erg s^{-1})	$E_{\rm X,all}$ (erg)
050502B	$(5.11 \pm 0.82)\times 10^{4}$	6.64 ± 0.92	$(8.30 \pm 0.27)\times 10^{49}$	$(4.87 \pm 0.79)\times 10^{45}$	$(1.27 \pm 0.41)\times 10^{51}$
050724	$(8.11 \pm 0.97)\times 10^{4}$	29.38 ± 3.40	$(1.42 \pm 0.15)\times 10^{48}$	$(2.19 \pm 0.35)\times 10^{43}$	$(3.39 \pm 0.42)\times 10^{48}$
050916	$(2.04 \pm 0.23)\times 10^{3}$	87.70 ± 26.96	$(1.56 \pm 0.07)\times 10^{50}$	$(2.30 \pm 0.28)\times 10^{47}$	–
130925A	$(0.58 \pm 0.03)\times 10^{3}$	15.71 ± 0.48	$(1.62 \pm 0.06)\times 10^{49}$	$(3.74 \pm 0.22)\times 10^{46}$	$(2.52 \pm 0.06)\times 10^{50}$
070318	$(8.71 \pm 5.41)\times 10^{4}$	3.96 ± 0.63	–	–	–
070429A	$(8.65 \pm 2.12)\times 10^{4}$	3.28 ± 0.78	–	–	–
150626B	$(1.18 \pm 0.18)\times 10^{4}$	50.63 ± 2.34	–	–	–